ELSEVIER

Biophysical Chemistry 62 (1996) 95–108

Biophysical Chemistry

Theoretical basis for differential scanning calorimetric analysis of multimeric proteins

Danilo Milardi, Carmelo La Rosa, Domenico Grasso *

Dipartimento di Scienze Chimiche, Università di Catania, V. le A. Doria, 6-95125 Catania, Italy

Received 15 March 1996; accepted 28 May 1996

Abstract

A new general equation simulating irreversible DSC transitions of multimeric proteins was developed.

The equation put forward here is the result of an improved mathematical re-elaboration of the classical Lumry-Eyring models, where no restrictive a priori assumptions are made on the kinetic constraints of the denaturation process, or on the enthalpy of the final denatured state.

In order to test the wide applicability of this new effective theoretical tool, a series of DSC transitions were simulated with the aim of determining the effects of all relevant thermodynamic, kinetic or experimental parameters on the shape of DSC profiles.

Moreover, the classical equations used widely in DSC investigations for the calculus in both kinetic parameters and changes of molecularity, were studied in the light of the model developed here, highlighting, in each case, their rather limited applicability.

The new approach proposed in this article was applied to study the thermal denaturation of an hexameric protein (Glucosamine-6-phosphate deaminase), putting in evidence the practical applicability of the theorethical equations developed.

Keywords: Differential scanning calorimetric analysis; Multimeric proteins

1. Introduction

The study of protein folding/unfolding and stability is of paramount importance today both in the academic field and in biotechnology. With the build-up of structural information concerning proteins, we have become increasingly convinced that protein structures are, both in the solid state and in solution, extremely sophisticated and precise. However, when considering the fascinating models of proteins resulting from crystallographyc, NMR analysis and computer simulations the question does arise as to how stable real protein structures are. It is evident that with no answer to this question we cannot hope to solve the problem of the intramolecular interactions responsible for a given structure, i.e., the problem of assembling all the elements of a polypeptide into one system, this being called the native protein macromolecule. Without a quantitative definition of structure stability, discussions on the mechanism of struc-

* Corresponding author. E-mail: dgrasso@dipchi.unict.it, Tel.: 0039.95.339572, Fax.: 0039.95.580138.

PII S0301-4622(96)02191-6

ture organization from random polypeptide chains and on the mechanism of changes in this structure in relation to protein functioning are groundless [1,2].

Paradoxically, the stability of any structure can be judged by studying its destruction [3]. Thus, the transition from the native to the denatured state for many proteins has been followed using various techniques involving mainly the kinetic or the thermodynamic approach [4–11]. This transition has been achieved generally by denaturant agents, such as urea or guanidine hydrochloride, by changes in pH and/or ionic strength [12], or by temperature [13–16]. In this latter case, high-sensitivity Differential Scanning Calorimetry (DSC) is probably the most suitable technique for characterizing the thermal stability of proteins since it provides detailed information about the energetics and mechanism of reversible unfolding [17–25]. The above types of analysis are based on equilibrium thermodynamics and require that the experimental heat capacity data accurately reflect the equilibrium protein unfolding. The equilibrium criterion usually applied is the reproducibility of the DSC trace in a second heating of the sample, the so-called calorimetric reversibility [26].

Analysis of a variety of protein systems has shown that small (M.W. < 20000) globular proteins, in particular experimental conditions, usually undergo reversible, two-state thermally induced folding/unfolding transitions [2]. The situation is not the same for larger multidomain, metal or multisubunit proteins [27–33]. These cases cannot be studied directly in terms of equilibrium thermodynamics i.e. changes in entropy and Gibbs function cannot be extracted from the first Cp vs T trace. Nevertheless, it has been widely held in literature that irreversible alteration of the unfolded state does not significantly distort the DSC transitions, but takes place at a somewhat higher temperature [34–39]. This is equivalent to assuming that protein thermal stability is determined by equilibrium factors even when denaturation is irreversible overall. Recent experimental and theoretical works highly disfavour this claim: in fact, it has been shown that irreversible DSC transitions are somehow distorted by time-dependent factors [40–43].

A rigorous analysis of the calorimetric data obtained for systems exhibiting irreversible complex transitions must thus be based on the detailed theoretical modelling of transition kinetics. Success in this new, unorthodox, approach depends greatly on the correct choice of the kinetic model, and of course, on the wide availability of different models in literature.

The theoretical modelling of the irreversible unfolding of monomeric proteins is well established [40,43,44]. However, if we exclude the pioneering work of Sanchez-Ruiz [43], detailed theoretical studies on irreversible denaturation models of multimeric proteins are not available in literature. Here we present a theoretical study expressly devoted to simulating the DSC traces corresponding to the irreversible thermal unfolding of multimeric proteins. In particular, we have explored several situations with different kinetic constraints whilst taking into account the possibility of a not negligible thermal effect associated to the irreversible step.

We have also compared our new, general model with the previous, more approximated ones. This comparison has highlighted the fact that the applicability of previously developed theoretical models is restricted to particular kinetic situations only. In the present paper we have elucidated and quantified these limitations. Finally, in order to test the wide applicability of the model developed here, we have applied our new approach to an experimental case: Glucosamine-6-phosphate deaminase.

2. Theory

The theoretical model developed can be depicted in the following scheme:

$$N_n \overset{K}{\leftrightarrow} nU \overset{k}{\rightarrow} F$$

According to this model, the n-meric native protein N_n undergoes a two-state reversible unfolding with simultaneous dissociation into n monomers. The thus-obtained unfolded species U, instead, undergoes an irreversible alteration to yield a final state F. We assume that chemical equilibrium between species N_n and U is always established, that the difference between the heat capacity of unfolded and native state (ΔCp) is negligible, and that the irreversible step is a first-order kinetic process.

In these conditions, the equilibrium constant K is,

$$K = \frac{[U]^n}{[N_n]} \quad (1)$$

[U] and $[N_n]$ being the molar concentration of unfolded and native species respectively. The temperature-dependence of K can be expressed by the classical equation:

$$K = \exp\left[-\frac{\Delta H_U}{R} \cdot \left(\frac{1}{T} - \frac{1}{T_{1/2}} \right) \right] \quad (2)$$

where ΔH_U is the enthalpy change associated to the reversible process, the so-called 'unfolding enthalpy', and $T_{1/2}$ is the temperature at which $K = 1$.

We also assume that the rate constant k of the irreversible step changes with temperature according to the Arrhenius equation, which is used in the form:

$$k = \exp\left[-\frac{E}{R} \cdot \left(\frac{1}{T} - \frac{1}{T^*} \right) \right] \quad (3)$$

where E is the activation energy and T^* is the temperature at which $k = 1$ [the frequency factor is $\exp(E/RT^*)$]. The rate of formation of the final state F is given by the following kinetic equation:

$$\frac{dC_F}{dt} = k \cdot C_U \quad (4)$$

where C_F and C_U are the concentrations in mg ml^{-1} of the final and unfolded state respectively. The unfolding equilibrium constant K (Eq. (1)) can also be written in terms of mg ml^{-1} concentrations:

$$K = n \cdot M^{(1-n)} \frac{C_U^n}{C_N} \quad (5)$$

where M is the molecular weight of the monomer and C_N is the concentration of the native protein. If we combine Eq. (4) with Eq. (5), we obtain:

$$\frac{dC_F}{dt} = k_{app} \cdot C_N^{1/n} \quad (6)$$

this being:

$$k_{app} = k \cdot \left(\frac{K}{n} \right)^{1/n} \cdot M^{((n-1)/n)} \quad (7)$$

If we now indicate with C_t the total concentration (in mg ml^{-1}) of the protein, it will be at any temperature:

$$C_t = C_N + C_U + C_F \quad (8)$$

If we combine Eq. (5), (6) and (8), we obtain

$$-\frac{d}{dt}\left[\left(\frac{K}{n} \right)^{1/n} \cdot M^{((n-1)/n)} \cdot C_N^{1/n} \right] - \frac{dC_N}{dt} = k_{app} \cdot C_N^{1/n}. \quad (9)$$

In a DSC experiment, however, temperature changes with time according to a constant scanning rate $v = dT/dt$. Hence, by transforming time in temperature the relevant differential equation is:

$$\left(\frac{M^{(n-1)}}{n} \right)^{1/n} \cdot \frac{d}{dT}\left(K^{1/n} \cdot C_N^{1/n} \right) + \frac{dC_N}{dT} = -\frac{1}{v} k_{app} C_N^{1/n}. \quad (10)$$

Eq. (10) cannot be integrated analytically. The numerical integration of this differential equation was performed by means of a fourth-order Runge–Kutta algorithm from a low temperature T_0 (at which the rate is negligible and $C_N = C_t$) to a temperature T, leading to the temperature dependence of C_N, C_U and C_F. Finally, the excess heat capacity (C_p^{ex}) profile can be simulated based on the following:

$$C_p^{ex} = \frac{\Delta H_U}{C_t} \cdot \frac{dC_U}{dT} + \frac{\Delta H_F}{C_t} \cdot \frac{dC_F}{dT} \quad (11)$$

where ΔH_F is the enthalpy of the final state F (taking N as the reference state).

3. Results and discussion

The solutions of Eq. (5), (8) and (10) simulate the trend of C_N, C_U and C_F in the investigated temperature range. Eq. (11) can be used to simulate the C_p^{ex} vs T profiles relative to the thermal denaturation of a multimeric protein. These profiles depend on the following parameters: (1) the oligomerization state of the protein (n); (2) the unfolding enthalpy (ΔH_U); (3) the temperature at which the equilibrium constant approaches unity $T_{1/2}$; (4) the activation energy of the irreversible step (E); (5) the temperature at

which the kinetic constant approaches unity (T^*); (6) the enthalpy of the final state (ΔH_F); (7) the heating rate (v) and (8) the total protein concentration (C_t). The last two parameters, C_t and v, can be changed in a DSC experiment, while all the others n, ΔH_U, $T_{1/2}$, E, T^*, depend on the physical-chemical properties of the investigated protein. In order to simplify the calculations, we will refer to the appartent activation energy (E_{app}) of the process, rather than to E; these two quantities are bounded by the relationship: $E_{app} = E + \Delta H_U/n$.

The main problem in the simulation of the C_p^{ex} vs T profiles is that of clarifying to what extent the irreversible step overlaps the reversible unfolding. In Fig. 1 we report the relative populations of states N, U and F, calculated by means of the equations developed in the Theory section, in the temperature range 325–350 K. Three different kinetic situations have been considered each reported in the three panels of Fig. 1. In particular, Fig. 1(a) refers to a kinetic situation in which the frequency factor $\{\exp(E/RT^*)\}$ of the irreversible step, compared

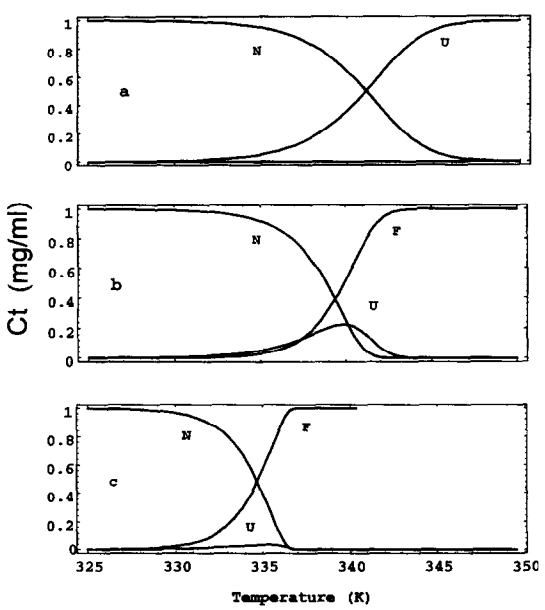

Fig. 1. Concentrations (in mg ml^{-1}) of the states N, U and F vs. T corresponding to the DSC transitions of a dimer. The profiles were calculated using Eqs. (5), (8) and (10), and the following parameters: $\Delta H_U = 800\,kJ\,mol^{-1}$, $E_{app} = 600\,kJ\,mol^{-1}$, $T_{1/2} = 353\,K$, $M = 15000$, $C_t = 1\,mg\,ml^{-1}$, $v = 2\,K\,min^{-1}$, $T^* = 355\,K$ (panel a), $T^* = 340\,K$ (panel b), $T^* = 335\,K$ (panel c).

with the position of the reversible process, is high, ($T^* \gg T_{1/2}$). In this case the kinetically-controlled process proceeds at a significant rate only at a temperature above the reversible unfolding; the two processes are well separated in the thermograms and the first calorimetric trace differs little from that corresponding to the reversible unfolding. Hence, the direct application of equilibrium thermodynamics is possible. Many papers dealing with the thermodynamic analysis of this situation are available in literature [23–46].

However, if the frequency factor is low ($T^* \ll T_{1/2}$), the irreversible step is fast at temperatures well below $T_{1/2}$. In this case the T_m value (temperature corresponding to the maximum heat capacity) is several degrees lower than that of the reversible unfolding, and only states N and F are significantly populated (path N → F) [7,26,33]. This kinetic situation is depicted in Fig. 1(c). In the intermediate situation (Fig. 1(b)), the irreversible step is fast in the temperature range of the reversible unfolding, nevertheless, the unfolded state U is significantly populated during the transition. The DSC profile deviates clearly from that corresponding to the equilibrium unfolding, and direct application of equilibrium thermodynamics would lead to significant errors. There exists, however, a significant amount of unfolded state in equilibrium with the native state during temperature-induced denaturation; that is, the calorimetric transition contains thermodynamic information about the reversible unfolding, which could be obtained through previously developed appropriate data analysis [7].

The present article is expressly devoted to developing the mathematical background for a detailed theoretical description of this intermediate (and more realistic) kinetic situation for DSC scans of multisubunit proteins.

In the following subsections we will elucidate the effect of each of the parameters which appear in Eq. (11) on the shape of the DSC profile. For the sake of clarity, we have chosen a set of 'standard' parameters, i.e. $n = 2$, $\Delta H_U = n^* 400\,kJ\,mol^{-1}$, $\Delta H_F = n^* 400\,kJ\,mol^{-1}$, $E_{app} = 600\,kJ\,mol^{-1}$, $M = 15000$, $C_t = 1\,mg\,ml^{-1}$, $T_{1/2} = 353.15\,K$, $T^* = 340.15\,K$. In the simulation of the curves, a single parameter will be changed, while all the other will be kept equal to the 'standard' values.

3.1. Effects of T^*, $T_{1/2}$, and E_{app} on the shape of DSC thermograms

The first two parameters (T^* and $T_{1/2}$) are related to the relative positions of the unfolding equilibrium and the kinetic step. The apparent activation energy E_{app} determines the rate of the irreversible step. In Fig. 2 the effect of T^* on the C_p^{ex} profiles is reported. It can be noted that when T^* increases, the irreversible step becomes fast only at high temperatures, and the shape of the curve is not distorted. In this case the situation is that reported in Fig. 1(a), where the thermodynamic equilibrium between states N and U is clearly depicted by the DSC peak. The effect of $T_{1/2}$ (see Fig. 3) is the opposite; when $T_{1/2}$ increases the shape of the peak is more distorted because the equilibrium step is placed nearer the kinetically-controlled process.

The effect of the apparent activation energy is reported in Fig. 4. When E_{app} increases, the irreversible step slackens but its frequency factor remains unchanged. Nevertheless, the position of the peak (T_m) moves towards the high temperature side of the thermograms. At increasing E_{app}, the asymmetry and the sharpness of the peak increase.

3.2. Effect of the enthalpy of the final state

If we take N as the reference state, the heat of the process of aggregation (U → F) ΔH_{ag} is bound to the enthalpy of the final state (ΔH_F) by the following relationship: $\Delta H_{ag} = \Delta H_U - \Delta H_F$. In Fig. 5 we report the effect of the heat of aggregation in the case of a dimeric protein. From this figure we can note that at decreasing ΔH_F, T_m of the endothermic curve does not change, while the exothermic peak at the end of the curve and obviously the calorimetric enthalpy both decrease. For such curves the correct calculation of the unfolding enthalpy is impossible if calorimetric data are not considered adequately.

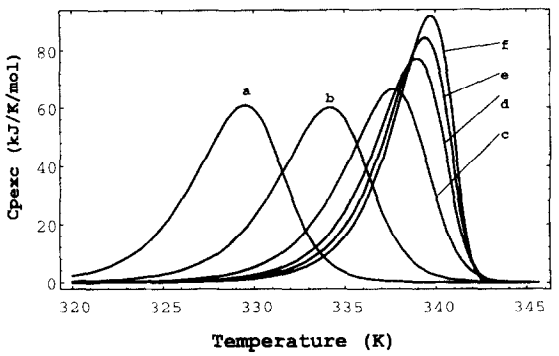

Fig. 3. Effect of $T_{1/2}$ on DSC transitions predicted by Eq. (11) and the following parameters: $n = 2$, $\Delta H_U = n^* 400\,kJ\,mol^{-1}$, $E_{app} = 600\,kJ\,mol^{-1}$, $\Delta H_F = n^* 400\,kJ\,mol^{-1}$, $M = 15000$, $C_t = 1\,mg\,ml^{-1}$, $v = 2\,K/min$, $T_{1/2} = 340\,K$ (curve a), $T_{1/2} = 345\,K$ (curve b), $T_{1/2} = 349\,K$ (curve c), $T_{1/2} = 351\,K$ (curve d), $T_{1/2} = 352\,K$ (curve e), $T_{1/2} = 353\,K$ (curve f).

3.3. The experimental parameters: effect of C_t and v

These two parameters are very important for one simple reason: they are not bound to the nature of

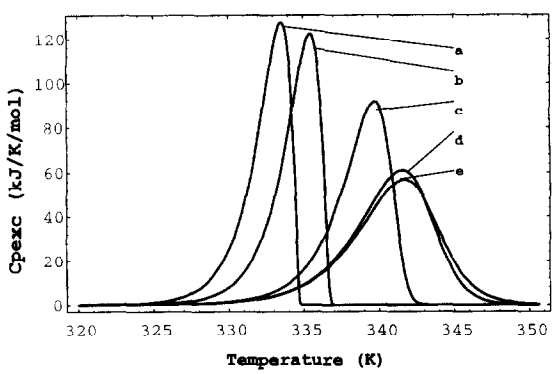

Fig. 2. Effect of T^* on DSC transitions predicted by Eq. (11) and the following parameters: $n = 2$, $\Delta H_U = n^* 400\,kJ\,mol^{-1}$, $E_{app} = 600\,kJ\,mol^{-1}$, $\Delta H_F = n^* 400\,kJ\,mol^{-1}$, $M = 15000$, $C_t = 1\,mg\,ml^{-1}$, $T_{1/2} = 353\,K$, $v = 2\,K\,min^{-1}$, $T^* = 333\,K$ (curve a), $T^* = 335\,K$ (curve b), $T^* = 340\,K$ (curve c), $T^* = 345\,K$ (curve d), $T^* = 350\,K$ (curve e).

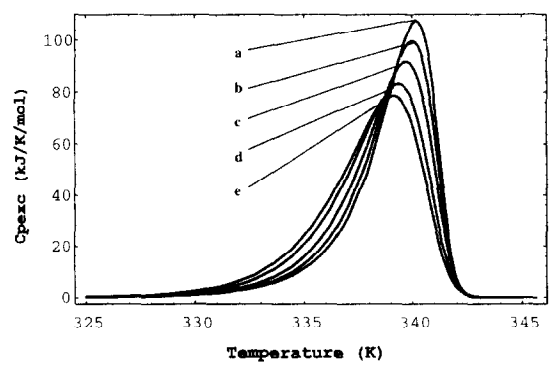

Fig. 4. Effect of E_{app} on DSC transitions predicted by Eq. (11) and the following parameters: $n = 2$, $\Delta H_U = n^* 400\,kJ\,mol^{-1}$, $\Delta H_F = n^* 400\,kJ\,mol^{-1}$, $T^* = 340\,K$, $M = 15000$, $C_t = 1\,mg\,ml^{-1}$, $v = 2\,K\,min^{-1}$, $E_{app} = 800\,kJ\,mol^{-1}$ (curve a), $E_{app} = 700\,kJ\,mol^{-1}$ (curve b), $E_{app} = 600\,kJ\,mol^{-1}$ (curve c), $E_{app} = 500\,kJ\,mol^{-1}$ (curve d), $E_{app} = 450\,kJ\,mol^{-1}$ (curve e).

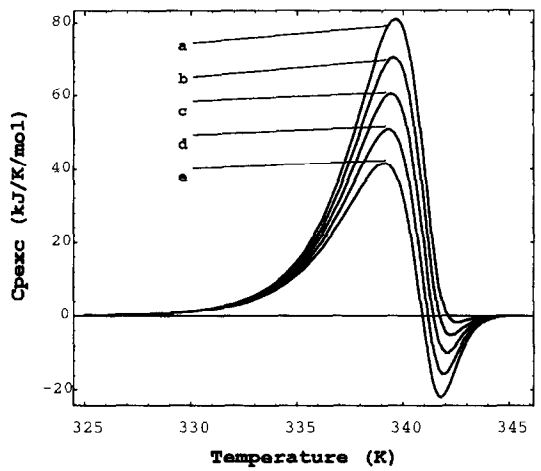

Fig. 5. Effect of ΔH_F on DSC transitions predicted by Eq. (11) and the following parameters: $n = 2$, $\Delta H_U = n^* 400\,kJ\,mol^{-1}$, $E_{app} = 600\,kJ\,mol^{-1}$, $T_{1/2} = 353\,K$, $T^* = 340\,K$, $M = 15000$, $v = 2\,K\,min^{-1}$, $C_t = 1\,mg\,ml^{-1}$, $\Delta H_F = n^* 350\,kJ\,mol^{-1}$ (curve a), $\Delta H_F = n^* 300\,kJ\,mol^{-1}$ (curve b), $\Delta H_F = n^* 250\,kJ\,mol^{-1}$ (curve c), $\Delta H_F = n^* 200\,kJ\,mol^{-1}$ (curve d), $\Delta H_F = n^* 150\,kJ\,mol^{-1}$ (curve e).

the protein and can be experimentally programmed. For this reason the effects of these two parameters on the shape of the C_p^{ex} profiles are extremely important as they can suggest the right choice of experimental variables in order to obtain a DSC curve as suitable as possible for thermodynamic analysis.

Fig. 6 shows the effect of scan rate for a dimeric protein in the kinetic situation of Fig. 1(b). As it can be noted, the asymmetry of the curve decreases with increasing scan rate and the shape of the curve becomes more and more similar to the two-state equilibrium model. In principle, it should be possible to obtain thermodynamic information even in the case of a rate-dependent DSC trace as it has previously been done [42,48]. We must highlight, however, that the extrapolation of DSC curves at infinite scan rate has to be carried out with great care, as the time response of the best commercial micro-calorimeters prevents the obtaining of realistic data beyond scan rates of $1.3\,°C\,min^{-1}$. This argumentation is even more evident if we consider the possibility of a non-negligible thermal effect associated to the irreversible step. This situation is depicted in Fig. 7. At increasing scan rates the endothermic peak becomes

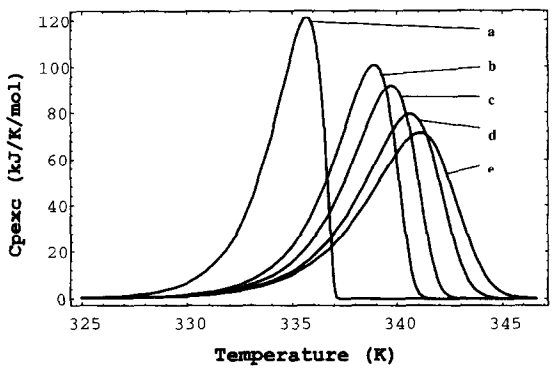

Fig. 6. Effect of scan rate on DSC transitions predicted by Eq. (11) and the following parameters: $n = 2$, $\Delta H_U = n^* 400\,kJ\,mol^{-1}$, $\Delta H_F = n^* 400\,kJ\,mol^{-1}$, $E_{app} = 600\,kJ\,mol^{-1}$, $T_{1/2} = 353\,K$, $T^* = 340\,K$, $M = 15000$, $C_t = 1\,mg\,ml^{-1}$, $v = 0.1\,K\,min^{-1}$ (curve a), $v = 1\,K\,min^{-1}$ (curve b), $v = 2\,K\,min^{-1}$ (curve c), $v = 5\,K\,min^{-1}$ (curve d), $v = 10\,K\,min^{-1}$ (curve e).

less sharp and approximates to a two-state equilibrium model, while the exothermic peak shifts towards a higher temperature. This situation is similar to that observed in the case of monomeric proteins [40].

The effect of the total protein concentration C_t is reported in Fig. 8. It should be noted that T_m depends on the total protein concentration as reported in literature to date [43]. This effect is evident if we

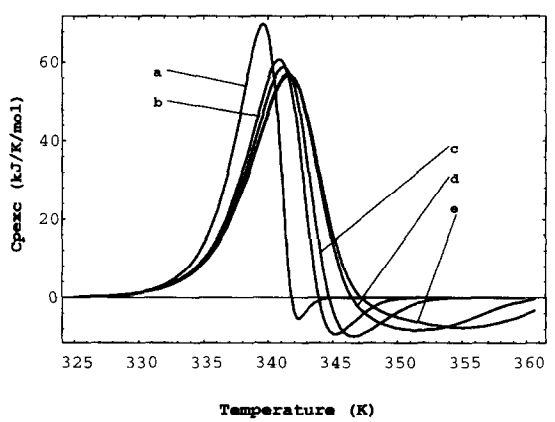

Fig. 7. Effect of scan rate on DSC transitions predicted by Eq. (11) in the case of a non-negligible exothermic effect associated to the irreversible step. The parameters used are: $n = 2$, $\Delta H_U = n^* 400\,kJ\,mol^{-1}$, $\Delta H_F = n^* 400\,kJ\,mol^{-1}$, $E_{app} = 600\,kJ\,mol^{-1}$, $T_{1/2} = 353\,K$, $T^* = 340\,K$, $M = 15000$, $C_t = 1\,mg\,ml^{-1}$, $v = 0.1\,K\,min^{-1}$ (curve a), $v = 0.5\,K\,min^{-1}$ (curve b), $v = 1\,K\,min^{-1}$ (curve c), $v = 5\,K\,min^{-1}$ (curve d), $v = 10\,K\,min^{-1}$ (curve e).

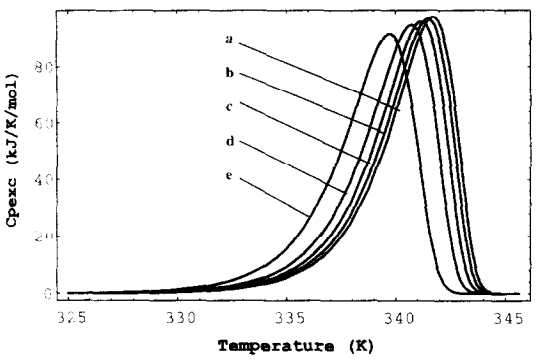

Fig. 8. Effect of C_t on DSC transitions predicted by Eq. (11) and the following parameters: $n = 2$, $\Delta H_U = n^* 400\,kJ\,mol^{-1}$, $\Delta H_F = n^* 400\,kJ\,mol^{-1}$, $E_{app} = 600\,kJ\,mol^{-1}$, $T_{1/2} = 353\,K$, $T^* = 340\,K$, $M = 15000$, $v = 2\,K\,min^{-1}$, $C_t = 1\,mg\,ml^{-1}$ (curve a), $C_t = 3\,mg\,ml^{-1}$ (curve b), $C_t = 5\,mg\,ml^{-1}$ (curve c), $C_t = 7\,mg\,ml^{-1}$ (curve d), $C_t = 9\,mg\,ml^{-1}$ (curve e).

consider the fact that any factor that 'displaces' the preliminary equilibrium will affect the rate of formation of the final state. Thus, increasing the total protein concentration gives rise to a lower fraction of the unfolded (or intermediate) state, a lower rate of formation of the final state, and a consequent shift of the DSC transitions to lower temperatures.

3.4. Effect of n on the shape of C_p^{ex} vs. T profile

A series of DSC profiles relative to the thermal denaturation of multimeric proteins for the kinetic situation described in Fig. 1(b) were simulated for different oligomerization states n, and reported in Fig. 9. As it can be noted, the position of T_m is strongly influenced by molecularity n. In particular when n increases, T_m moves towards the low temperature side of the thermogram. The sharpness of the peaks has an irregular trend. It remains unchanged for $n = 1$ and $n = 2$, decreases for $n = 3$ and then increases for $n = 4$, 5 and 6. This behavior is in open contrast with a previous study [43] which states the asymmetry of the peak as being more pronounced for the higher values of n. Moreover, the model reported in the paper concerned does not foresee any change in the position of the peak with increasing n. The model depicted by Sanchez-Ruiz, however, simply shows a particular case of what we have demonstrated in a general sense. In fact, when the set of unfolding parameters are chosen so that the unfolded state U is not populated during the unfolding, the behavior of the curves corresponds to the previsions of Sanchez-Ruiz [47].

In the following sections we will discuss, in the light of the new model put forward in this paper, the equations widely used for the calculus of apparent activation energy and molecularity. The principal aim in this kind of analysis is to evaluate the limits of applicability of these equations.

3.5. Applicability of classical equations for the calculus of E_{app} and n

The solution of Eq. (10), as we have previously underlined, is not analytical, but only numerical. It can thus be extremely difficult to extract from this model new mathematical equations correlating directly kinetic and/or thermodynamic parameters with the calorimetric data. Nevertheless, our model can be considered a very useful tool for elucidating the limits of the equations previously reported in literature. Moreover, it is possible from this analysis to suggest the best experimental conditions for the widest applicability of the investigated equations.

Mathematical elaboration of model (a) in the kinetic situation of Fig. 1(c) leads to several useful relationships that give:

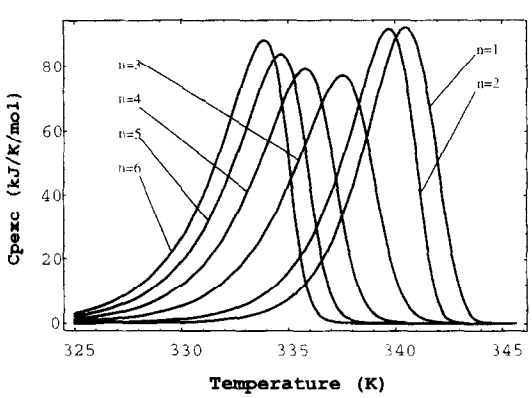

Fig. 9. Effect of the oligomerization state n on DSC transitions predicted by Eq. (11) and the following parameters: $\Delta H_U = n^* 400\,kJ\,mol^{-1}$, $\Delta H_F = n^* 400\,kJ\,mol^{-1}$, $E_{app} = 600\,kJ\,mol^{-1}$, $T_{1/2} = 353\,K$, $T^* = 340\,K$, $M = 15000$, $C_t = 1\,mg\,ml^{-1}$, $v = 2\,K\,min^{-1}$. The numbers alongside the transitions stand for the oligomerization state considered during the simulations.

(a) the scanning rate effect on T_m (at constant C_t) [26,43]:

$$\ln\left(\frac{v}{T_m^2}\right) = -\frac{E_{app}}{RT_m} + c, \qquad (12)$$

(b) the effect of the total protein concentration on the temperature corresponding to maximum heat capacity (at constant scanning rate) [43,48]:

$$\frac{E_{app}}{RT_m} - 2\ln T_m + \frac{n-1}{n}\ln C_t = \text{const} \qquad (13)$$

Eq. (12) states that, if the irreversible step occurs too fast to allow the unfolded state to be significantly populated during the thermally induced transition, the slope of a linear plot of $\ln(v/T_m^2)$ values vs $1/T_m$ would lead to the apparent activation energy (E_{app}) of the process. However, the straightforward application of Eq. (12) in the kinetic situation of Fig. 1(b), can lead to gross errors.

In order to clarify these fundamental points, we have simulated a series of DSC experiment by means of Eq. (11) and the set of 'standard parameters' previously reported. Scan rate only will be changed (see Fig. 6) and the values of T_m are reported in a linear plot of ln (B) where $B = v/T_m^2$ vs $1/T_m$ (see Fig. 10). In this case linear regression analysis shows an acceptable value of the correlation coefficient ($R = 0.986$), but the estimated slope of the plot predicts an E_{app} of 793 kJ mol^{-1}. If compared with the expected 600 kJ mol^{-1}, this value can be considered only as a rough approximation. It is clear that the variations of the unfolding parameters in the sense of a less populated state U would lead to a better correspondence between results and expectations. In fact the points of the plot obtained at lower scan rates (less populated state U) correspond better with Eq. (12). In other words, if one attempts to calculate kinetic parameters from the effect of scan rate on the position of the peak, the use of low scan rate leads to better results. In the case of a non-negligible exothermal effect associated to the irreversible step, expectations concerning Eq. (12) and actual experimental data correspond even less. This can be noted in Fig. 11. In this case the calculated value of E_{app} is 1709 kJ mol^{-1} and if compared to the expected value of 600 kJ mol^{-1}, is evident that Eq. (12) cannot be used to calculate kinetic parameters.

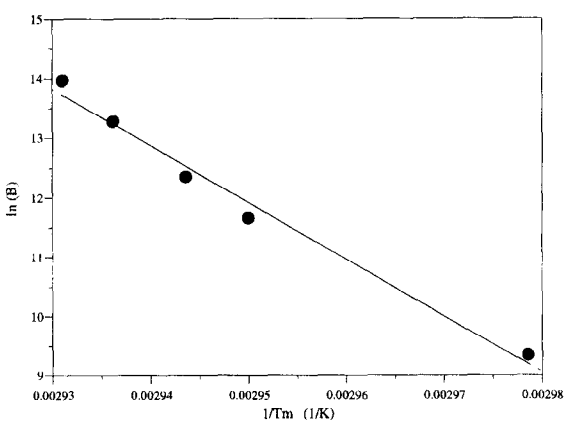

Fig. 10. Plot of $\ln(B)$ where $B = V/T_m^2$ vs $1/T_m$ for the DSC transitions of Fig. 6. The slope of the straight line (correlation coefficient of the linear regression 0.986) is not the same predicted by Eq. (12) (see the text for further details).

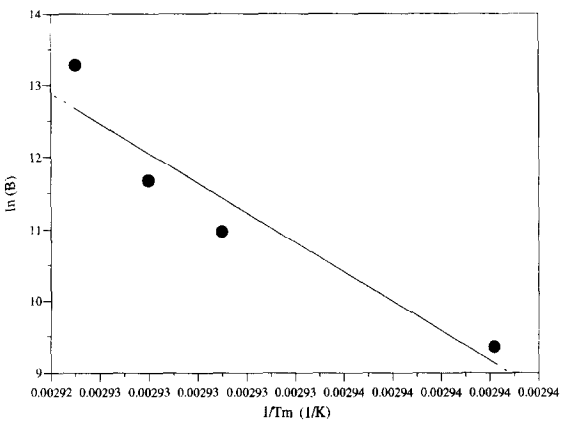

Fig. 11. Plot of ln B (where $B = V/T_m^2$) vs $1/T_m$ for the DSC transitions of Fig. 7. The exothermic effect associated with the irreversible step negatively influences the calculus of the apparent activation energy. The slope of the straight line (correlation coefficient 0.901) is far from the predictions of Eq. (12) (see the text for further details).

Eq. (13) allows the calculation of the oligomerization state n of the protein from the effect of the total protein concentration C_t on the position of T_m. As in Eq. (12), Eq. (13) was built up starting from the approximation of a negligible population of state U. For realistic values of E_{app} the term $2\ln T_m$ changes with T_m much more slowly than does the term E_{app}/RT_m; hence the term $2\ln T_m$ can be taken as a constant and, therefore, Eq. (13) predicts that a plot

of $\ln C_t$ vs $1/T_m$ should be linear with a slope equal to $-n^* E_{app}/((n-1)R)$.

It is also necessary to bear in mind that for the simple equilibrium model $N_n \Leftrightarrow nU$, equilibrium thermodynamics predicts, that T_m increases with C_t according to the equation [45]:

$$\Delta H_{VH}/RT_m + (n-1)\ln C_t = \text{const} \qquad (14)$$

where ΔH_{VH} is the so-called Van't Hoff enthalpy, which can be calculated according to the equation:

$$\Delta H_{VH} = A \cdot R \cdot T_m^2 \cdot C_{p,m}^{ex}/\Delta H \qquad (15)$$

where C_{pm}^{ex} and ΔH are the maximum excess heat capacity and the denaturation enthalpy respectively (values of A for several values of n are given by Manly and Sturtervant [34]).

It is to be noted that the protein concentration effects predicted by Eq. (13) and Eq. (14) are similar. It is thus foreseable that even in an intermediate kinetic situation plots of ln C_t vs $1/T_m$ should be linear. This prediction is correct as we can see from Fig. 12, but the calculus of n (2.4) from the slope of the plot can be considered only a rough approximation of the expected 2.

In principle, the applicability of Eq. (13) does not depend on scan rate. This means that the values of n calculated by means of this equation should not change on changing the experimental scan rate of the DSC experiments. But, if applied to real cases, this claim must be considered with caution. In fact Eq. (13) and Eq. (14), were evaluated for two limit cases (C_U and C_F are alternately considered negligible). For this reason either Eq. (13) or Eq. (14) should not be influenced by the particular choice of v. But for most of the real cases, N, U, and F are all significantly populated in the investigated denaturation range. Hence it is foreseeable that the applicability of Eq. (13), depend greatly on the particular kinetic situation determined by the combination of all the kinetic parameters.

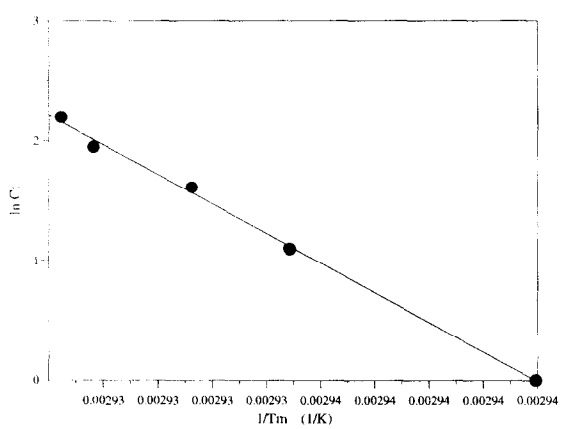

Fig. 12. Plot of ln C_t vs $1/T_m$ for DSC transitions of Fig. 8. The slope of the straight line (correlation coefficient 0.987) obtained using Eq. (13), gives a predicted change of molecularity $n = 2.4$ (see the text for details).

Table 1
The values of the oligomerization state n calculated by means of Eq. (13), at different scan rates. These values were calculated from the corresponding DSC transitions predicted by Eq. (11) and the following parameters: $\Delta H_U = n^* 400\,\text{kJ mol}^{-1}$, $\Delta H_F = n^* 400\,\text{kJ mol}^{-1}$, $E_{app} = 600\,\text{kJ mol}^{-1}$, $T_{1/2} = 353\,\text{K}$, $T^* = 340\,\text{K}$, $M = 15000$, $C_t = 1\,\text{mg ml}^{-1}$, $n = 2$ (second column), $n = 3$ (third column)

Scan rate v	$n = 2$ (expected)	$n = 3$ (expected)
$0.1°\text{C m}^{-1}$	2.04	4.03
$0.5°\text{C m}^{-1}$	2.17	7.31
$1°\text{C m}^{-1}$	2.27	10.48
$2°\text{C m}^{-1}$	2.42	18.45
$3°\text{C m}^{-1}$	2.57	-
$5°\text{C m}^{-1}$	2.78	-

In order to highlight this behavior, we have calculated the values of n from Eq. (13) at different scan rates keeping all the other parameters constant i.e. $\Delta H_U = n^* 400\,\text{kJ mol}^{-1}$, $\Delta H_F = n^* 400\,\text{kJ mol}^{-1}$, $E_{app} = 600\,\text{kJ mol}^{-1}$, $T_{1/2} = 353\,\text{K}$, $T^* = 341\,\text{K}$, $n = 2$. These results are reported in Table 1.

As we can note, correspondence between expected and calculated values is greater when v decreases. This was foreseeable if we consider that Eq. (13) was built in consideration of negligible values of C_U. As C_U increases with scan rate, it is clear that in this case correspondence is weaker. Obviously, all modifications of the parameters that make the state U less populated make the predictions of Eq. (13) more realistic.

Moreover, the applicability of Eq. (13) gets worse for higher values of n (see 3rd column of Table 1 calculated for $n = 3$). In this case the application of Eq. (13) can lead to unacceptable errors.

3.6. Calculus of the van't Hoff enthalpy from the shape of the curve

The Van't Hoff enthalpy is a very important parameter in the DSC analysis of proteins [46]: it provides a useful tool to test the validity of the two-state model for the investigated transition as it must approach the unity in the case of only two states populated.

As a consequence, it is remarkably influenced by the occurrence of kinetically-controlled steps. We have investigated the effect of several parameters on ΔH_{VH} values for $n = 2$, and the results are reported in Table 2. We shall indicate with r the so-called Van't Hoff ratio: $r = \Delta H/\Delta H_{VH}$ that can be calculated from Eq. (15).

The values reported in Table 2 were obtained from the simulated curves of Figs. 2–9.

The values of Table 2(A), report the trend of the Van't Hoff ratio when T^* (i.e. the frequency factor of the irreversible step) increases when all other parameters are constant. It can be noted that r increases with increasing T^*. This behavior can be understood if we hold in mind that when T^* increases the irreversible step takes place at higher scan rate: this mean that DSC traces are less distorted with respect to the two-state model and r is closer to unity.

An opposite situation is depicted in Table 2(B). In this case the values of $T_{1/2}$ are increased keeping constant all other parameters. When $T_{1/2} \ll T^*$, r is very close to unity. In fact, in these conditions the reversible unfolding takes place before the irreversible step, and the two processes do not overlap. On the contrary when $T_{1/2}$ increases the irreversible step and reversible unfolding occur simultaneously and the DSC profile is distorted (T_m is placed before $T_{1/2}$); as a consequence, r decreases.

Table 2(C) describes the effect of the apparent activation energy on the value of r. As we have yet pointed out on discussing Fig. 4, apparent activation energy influences the rate of the irreversible step, but not its relative position (determined by T^*). However, when E_{app} increases, the irreversible step slackens and r is closer to unity. In Table 2(D) the effect of the heat of aggregation on r is reported. As expected, on increasing values of the heat of aggregation, (and as a consequence on decreasing ΔH_F) the values of r decreases dramatically. This effect is much more evident than for any other parameter.

In other words, the heat of aggregation can make (more than any other parameter) the Van't Hoff analysis of the DSC curve, unreliable. In this sense, the distortions caused by the exothermal effects are the most harmful.

As we have yet pointed out, the experimental scanning rate can influence considerably the shape of the DSC curves, and as a consequence the Van't Hoff ratio. This situation is depicted in Table 2(E), where the effect of v on the values of r is reported. As v increases, the state U becomes more populated and the shape of the DSC curve is more similar to the two-state reversible unfolding model (r is closer to unity). A similar situation is described in Table 2(F); but in this case an exothermal effect ($-100\,kJ\,mol^{-1}$) associated with the irreversible step distorts the DSC curve. In the end, Table 2(G) describes the effect of total protein concentration on the value of r. It is interesting to note that when C_t increases the Van't Hoff ratio become smaller. This is because of the increasing rate of the irreversible step on increasing total protein concentration as pre-

Table 2
Effect of the unfolding parameters on the Van't Hoff ratio r calculated by means of Eq. (15) and the corresponding DSC transitions of Figs 2–9. The effects of T^*, $T_{1/2}$, E_{app}, ΔH_F, v (considering negligible the enthalpy difference between the final and the unfolded state), v (in this case $\Delta H_F = n^* 300\,kJ\,mol^{-1}$) and C_t, are reported in columns A, B, C, D, E, F, G, respectively

A		B		C		D		E		F		G	
T^*	r	$T_{1/2}$	r	E_{app}	r	ΔH_F	r	v	r	v	r	C_t	r
333	0.46	340	1.00	800	0.73	700	0.55	0.1	0.48	0.1	0.47	1	0.62
335	0.48	345	0.98	700	0.68	600	0.46	1	0.57	0.5	0.53	3	0.60
340	0.62	349	0.87	600	0.62	500	0.37	2	0.62	1	0.55	5	0.59
345	0.94	351	0.74	500	0.58	400	0.28	5	0.72	5	0.56	7	0.58
350	0.95	352	0.68	450	0.53	300	0.19	10	0.81	10	0.56	9	0.57

dicted by kinetic equations reported in the preceding subsection.

3.7. Calculus of E_{app} from the shape of the curve

Eq. (13) is not the only way to calculate the apparent activation energy of the process; it could be also extracted from the parameters corresponding to the maximum of the transition [43]:

$$E_{app} = n^{n/(n-1)} \cdot R \cdot T_m^2 \cdot C_{p,exc}^m / \Delta H. \quad (16)$$

Eq. (16), which has been developed for a process where the population of the state U is negligible, is of course influenced by all the parameters modifying the kinetic constraints.

In order to explore the applicability of Eq. (16) on changing the unfolding parameters, the values of E_{app} obtained from Eq. (16) and the simulated curves of Figs. 2–9 have been compared with the expected value of E_{app} used in the calculations. The results of this analysis, expressed as percentage errors, are reported in Table 3. The first interesting point highlighted by Table 3, is the negative sign of all the errors $E\%$ ($E\% = (E_{app}^{calcualted} - E_{app}^{expected})/E_{app}^{expected}$). This means that Eq. (16) gives always smaller values than the expected.

In Table 3(A) the values of percentage errors $E\%$ as a function of T^* are reported. On increasing values of T^*, the error in the calculation of the apparent activation energy increases.

Table 3(B) reports the variations of the percentage error $E\%$ as a function of $T_{1/2}$. When $T_{1/2} \ll T^*$ the irreversible and reversible processes do not overlap and the DSC profile is more similar to the curve expected for the two-state model; in this case application of Eq. (16) is rather limited.

Table 3(C) reports the effects of the variation of the apparent activation energy on the applicability of Eq. (16). As it can be noted, when the apparent activation energy increases the irreversible step slackens and therefore applicability of Eq. (16) is more limited. Table 3(D) describes the influence of the heat of aggregation on the applicability of Eq. (16). Unexpectedly, when the exothermal heat of aggregation increases (and, as a consequence, enthalpy associated to the final state F ΔH_F decreases) the percentage error in the calculus of E_{app} decreases. This is a strange behavior because we would expect a larger distortion (and as a consequence a larger error in the calculus of E_{app}) of the DSC curve when ΔH_F decreases. In reality, when ΔH_F decreases the values of C_{pmax} i.e. the values of the maximum of the heat capacity, decreases; in contrast, the value of ΔH (the denominator of Eq. (16) also decreases. These two simultaneous effects contribute in an apparent improvement of reliability of Eq. (16). In other words Table 3(D) shows that, under particular kinetic constraints, the calculus of E_{app} from Eq. (16) can give good results; but it is important to understand that they can be obtained from a fortuitous combination of the kinetic constraints. In Table 3(E) the effect of the scan rate on the shape of C_p curves is reported. When scan rate is increased the error becomes larger. When an exothermal process distorts significantly the shape of DSC curves, the effect of scan rate is less evident (see Table 3(F)). In fact when v decreases the error in the calculus of E_{app} decreases but more slowly with respect to Table 3(E). In any case, the errors are larger than Table 3(E). Finally, in Table 3(G) the effect of the total protein concentration is reported. It can be noted that an increase in C_t causes larger

Table 3
Percentage errors ($E\% = (E_{app}^{calculated} - E_{app}^{expected})/E_{app}^{expected}$) in the calculus of the apparent activation energy by means of Eq. (16) and the simulated DSC transitions of Figs 2–9. In particular the effects of T^*, $T_{1/2}$, E_{app}, ΔH_F, v in the case of $\Delta H_1 = \Delta H_2$, v in the case $\Delta H_F = 600\,kJ\,mol^{-1}$, C_t, are reported in columns A, B, C, D, E, F, G respectively

A		B		C		D		E		F		G	
T^*	$E\%$	$T_{1/2}$	$E\%$	E_{app}	$E\%$	ΔH_F	$E\%$	v	$E\%$	v	$E\%$	C_t	$E\%$
333	−1%	340	−55%	800	−38%	350	−27%	0.1	−5%	0.1	−27%	1	−26%
335	−5%	345	−53%	700	−33%	300	−25%	1	−20%	0.5	−35%	3	−24%
340	−31%	349	−47%	600	−26%	250	−23%	2	−27%	1	−37%	5	−22%
345	−51%	351	−38%	500	−21%	200	−18%	5	−36%	5	−39%	7	−21%
350	−53%	352	−33%	450	−13%	150	−10%	10	−43%	10	−40%	9	−20%

errors in the calculus of E_{app}: this was foreseeable since an increase of C_t determines (as the irreversible step becomes faster) a decrease of C_U, and as a consequence, a better agreement between expected and calculated value.

3.8. Application to an experimental case: Glucosamine-6-phosphate Deaminase

In order to test the validity of the new approach developed in the present paper, we have re-considered a previously studied [49] multimeric protein.

Escherichia Coli Glucosamine-6-phosphate Deaminase (G6PD) is an hexamer made up of six identical subunits of 29.7 kDa each [50]. The structural characteristics of this enzyme, make it an interesting model for studying the influence of subunit interactions in the thermal behavior of proteins. A previous differential scanning calorimetric study of this enzyme, has put in evidence a complex, irreversible denaturation path. In the present paper we have interpreted the experimental heat capacity data carried out in the previous paper [49] in the light of the new approach developed here.

The effect of scan rate on the position of the calorimetric peaks gives, by means of Eq. (12), the apparent activation energy of the denaturation process. In Fig. 13 a linear plot of $\ln(v/T_m^2)$ vs T_m is reported. From the slope of the linear regression of

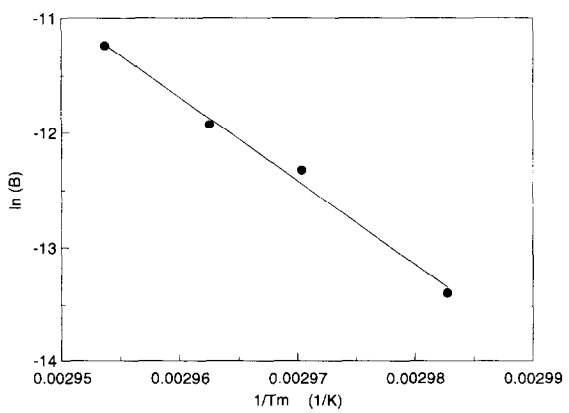

Fig. 13. Plot of ln B (where $B = V/T_m^2$) vs $1/T_m$ for the thermograms of G6PD. The experimental data of Ref. [49] were used for the calculations. The correlation coefficient of the linear regression is 0.991967. The apparent activation energy E_{app}, calculated from the slope of the plot is 605 kJ mol^{-1}.

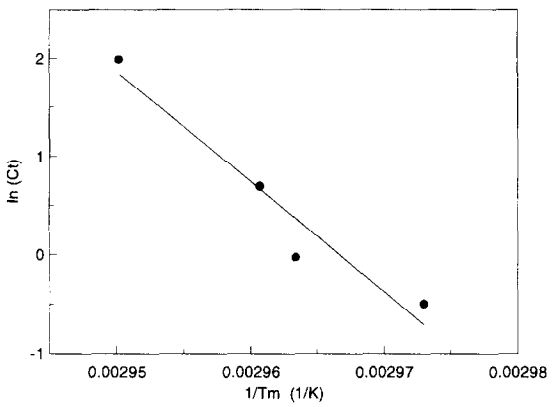

Fig. 14. Plot of $\ln C_t$ vs $1/T_m$ for the DSC transitions of G6PD reported in Ref. [49]. The correlation coefficient of the linear regression is 0.93618. The change of molecularity calculated from this plot is $n = 3$.

Fig. 13, we have calculated an apparent activation energy of 605 kJ mol^{-1}. However, the effect of protein concentration on the position of the calorimetric peaks, can be useful to calculate, by means of Eq. (13), the molecularity of the unfolding process. From the linear plot of ln C_t vs $1/T_m$ reported in Fig. 14 it is possible to calculate, for G6PD a molecularity of $n = 3$. In other words, the straightforward application of Eq. (12) and (13) to the case of G6PD has lead us to conclude that this enzyme unfolds with a simultaneous dissociation into dimers, and that the whole process is kinetically controlled with an apparent activation energy of 605 kJ mol^{-1}.

However, we have carried out a fit of an eperimental series of C_p data, by means of a Simplex algorithim, to minimize the function δ defined as:

$$\delta = \sqrt{\frac{\left(C_p(T)_{ex}^{theo}\right)^2 - \left(C_p(T)_{ex}^{exp}\right)^2}{\left(C_p(T)_{ex}^{exp}\right)^2}}$$

where $C_p(T)_{ex}^{theo}$ is the excess specific heat at given temperature calculated using Eq. (11) and $C_p(T)_{ex}^{exp}$ is the experimental excess specific heat curve reported in Ref. [49] (see Fig. 15). The minimization has given up the following results: $n = 2$, $\Delta H = 1058$ kJ mol^{-1}, $E_{app} = 450$ kJ mol^{-1}, $T^* = 348.15$ K, $T_{1/2} = 342.15$ K. It can be noted that the parameters calculated from the fit are different from the ones obtained from Eq. (12) and (13). In particular, the

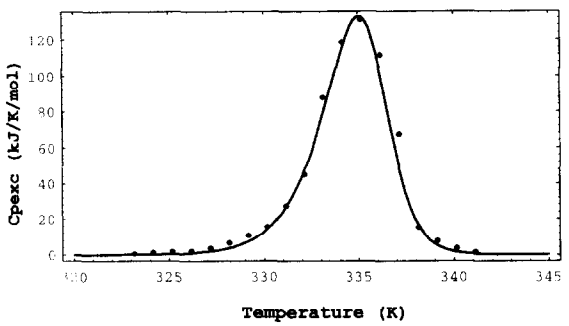

Fig. 15. Fit of the experimental data (see Ref. [49]) related to the thermal denaturation of G6PD with the equations developed in the text. The fit was carried out by means of a trial and error procedure. The optimized unfolding parameters are: $n = 2$, $\Delta H = 10580\,kJ\,mol^{-1}$, $v = 0.17\,K\,min^{-1}$, $C_t = 1\,mg\,ml^{-1}$, $M = 29700$, $T^* = 348.15\,K$, $T_{1/2} = 342.85\,K$.

different value of molecularity suggets that G6PD does not dissociates into dimers as calculated from Eq. (13), but into trimers.

4. Conclusions

The theroretical model developed in the present paper has elucidated many important aspects which have often been neglected in previous papers dealing with the DSC of proteins. First of all, it has been clearly shown that irreversible thermally-induced conformational transitions of multimeric proteins are regulated by a complex law which depends on many parameters. Some of these parameters (the total protein concentration and scanning rate) can be modified during a DSC experiment and their correct choice can determine the successful analysis of the DSC curves. Moreover, it has been shown that an acritical analysis of DSC curves both in terms of equilibrium thermodynamics and in terms of a totally irreversible process can be somewhat arbitrary. In fact, the possibility of a significantly populated unfolded state U even in the case of irreversible denaturation is not simply a theoretical hypothesis but, as several recent papers confirm, a real eventuality [42,48].

Therefore, the equations widely used for the calculus of molecularity and/or kinetic parameters, which were developed in the case of a very fast irreversible step ($C_U \approx 0$), represents only a limit case and do not give realistic results if applied in these intermediate situations.

This was also shown from a critical re-interpretation of the experimental C_p data for Glucosamine-6-phosphate-deaminase in the light of the new approach developed here.

Acknowledgements

This work was financially supported by italian MURST (Ministero della Università e della Ricerca Scientifica e Tecnologica), and CNR, Rome.

References

[1] C.R. Matthews, Annu. Rev. Biochem., 62 (1993) 653.
[2] P.L. Privalov, Adv. Prot. Chem., 33 (1979) 167.
[3] P.L. Privalov, Therm. Acta, 163 (1990) 33.
[4] K. Kuwajima, Proteins, 6 (1989) 87.
[5] T. Alber, Annu. Rev. Biochem., 58 (1989) 765.
[6] P.S. Kim and R.L. Baldwin, Annu. Rev. Biochem., 59 (1990) 631.
[7] E. Freire, W.W. Van Odsol, O.L. Mayorga and J.M. Sanchez-Ruiz, Annu. Rev. Biophys. Biophys. Chem., 19 (1990) 159.
[8] K.A. Dill, Biochemistry, 29 (1990) 7133.
[9] K.A. Dill and D. Shortle, Annu Rev. Biochem., 60 (1991) 795.
[10] J.M. Scholtz and R.L. Baldwin, Annu. Rev. Biophys. Biomol. Struct., 21 (1992) 95.
[11] F.X. Schmid, Annu. Rev. Biophys. Biomol. Struct., 22 (1993) 122.
[12] C. Tanford, Adv. Prot. Chem., 23 (1968) 121.
[13] A.M. Labhardt, J. Mol. Biol., 157 (1982) 331.
[14] K.C. Aune, A. Salahuddin, M.H. Zarlengo and C. Tanford, J. Biol. Chem., 242 (1967) 4486.
[15] C.R. Matthews and D.G. Westmoreland, Biochemistry, 14 (1975) 4532.
[16] P.A. Evans, K.D. Topping, D.N. Woolfson and C.M. Dobson, Proteins, 9 (1991) 248.
[17] P.L. Privalov and V.V. Plotnikov, Therm. Acta, 139 (1988) 257.
[18] P.L. Privalov and N.N. Khechinashvili, J. Mol. Biol., 86 (1974) 665.
[19] G.I. Makhatadze and P.L. Privalov, J. Mol. Biol., 232 (1993) 639.
[20] P.L. Privalov and G.I. Makhatadze, J. Mol. Biol., 232 (1993) 660.
[21] J.M. Sturtevant, Proc. Natl. Acad. Sci. USA, 74 (1977) 2236.
[22] G. Velicelebi and J.M. Sturtevant, Biochemistry, 18 (1979) 1180.

[23] P.L. Privalov and S.J. Gill, Adv. Prot. Chem., 39 (1989) 191.
[24] E. Freire and R.L. Biltonen, Biopolymers, 17 (1978) 463.
[25] R.L. Biltonen and E. Freire, CRC Crit. Rev. Biochem., 5 (1978) 85.
[26] J.M. Sanchez-Ruiz, J.L Lopez-Lacomba, M. Cortijo and P.L. Mateo, Biochemistry, 27 (1988) 648.
[27] A. Hernandez-Harana, A. Rojo-Dominguez, M.M. Altamirano and M.L. Calcagno, Biochemistry, 32 (1993) 3644.
[28] F. Conejero-Lara, P.L. Mateo, F.X. Aviles and J.M. Sanchez-Ruiz, Biochemistry, 30 (1991) 2067.
[29] M. Galisteo, P.L. Mateo and J.M. Sanchez-Ruiz, Biochemistry, 30 (1991) 2061.
[30] M. Guzman-Casado, A. Parody-Morreale, P.L. Mateo and J.M. Sanchez-Ruiz, Eur. J. Biochem., 188 (1990) 181.
[31] J.R. Lepock, A.M. Rodahl, C. Zhang, M.L. Heynen, B. Waters and K.H. Chang, Biochemistry, 29 (1990) 681.
[32] P.E. Morin, D. Diggs and E. Freire, Biochemistry, 29 (1990) 781.
[33] J.M. Sanchez-Ruiz, J.L Lopez-Lacomba, P.L. Mateo, M. Villanova, M.A. Serra and F.X. Aviles, Eur. J. Biochem., 176 (1988) 225.
[34] S.P. Manly, K.S. Matthews and J.M. Sturtevant, Biochemistry, 24 (1985) 3842.
[35] P.L. Privalov, Adv. Prot. Chem., 35 (1982) 1.
[36] P.L. Privalov and L.V. Medved, J. Mol. Biol., 159 (1982) 665.
[37] V. Edge, N.M. Allewell and J.M. Sturtevant, Biochemistry, 24 (1985) 5899.
[38] C.Q. Hu and J.M. Sturtevant, Biochemistry, 26 (1987) 178.
[39] C.Q. Hu and J.M. Sturtevant, Biochemistry, 28 (1989) 813.
[40] D. Milardi, C. La Rosa and D. Grasso, Biophys. Chem., 52 (1994) 183.
[41] D. Milardi, C. La Rosa and D. Grasso, Therm. Acta, 246 (1994) 183.
[42] C. La Rosa, D. Milardi, D. Grasso, R. Guzzi and L. Sportelli, J. Phys. Chem., 99 (1995) 14864.
[43] J.M. Sanchez-Ruiz, Biophys. J., 61 (1992) 921.
[44] R. Lumry R. and H. Eyring, J. Phys. Chem., 58 (1954) 110.
[45] K. Takahashi and J.M. Sturtevant, Biochemistry, 20 (1981) 6185.
[46] P.L. Privalov and S.A. Potekhin, Methods Enzymol., 131 (1986) 4.
[47] A.M. Klibanov and T.J. Ahern, in: Protein engineering, ed Oxenber D.L., Fox C.F., (New York: Liss 1983) p. 213.
[48] D. Grasso, C. La Rosa, D. Milardi and S. Fasone, Therm. Acta, 265 (1995) 163.
[49] A. Hernàndez-Arana, A. Rojo-Dominguez, M.M. Altamirano and M.L. Calcagno, Biochemistry, 32 (1993) 3644.
[50] M. Calcagno, P.J. Campos, G. Mulliert and J. Suastegui, Biochim. Biophys. Acta, 787 (1984) 165.